Heidelberg University

Institute of Computer Science

Visual Computing Group (VCG)

Master-Arbeit

Global Illumination Techniques for Tensor Field Visualization

Sebastian Bek

Matrikelnummer: 3481802

Betreuer: Sebastian Bek

Datum der Abgabe: 07.07.2019

Zusammenfassung

Tensorfelder werden meistens in Verbindung mit mechanischen Spanunngsverteilungen in 2D/3D-Gittern gebracht (vgl. Cauchy-Stress Tensor), haben aber auch andere praktische Bedeutungen in der Physik. Mithilfe von globalen Beleuchtungsmodellen/-techniken wird eine neue Methode entwickelt, um Tensorfelder zu visualisieren, die aber zusätzlich auch verwendet werden kann um die Lichtausbreitung in einer topologischen Szene zu beschreiben. Als Grundlage leiten wir ein einfaches Lichtausbreitungsschema für kartesische Gitter ab, dass die Prinzipien der Ausbreitungsdämpfung und Energieerhaltung beachtet und Licht-verteilung/en für gegebene Lichtquellenrichtung/en und -positionen bis zur Konvergenz approximieren kann. Als unterliegendes Modell werden die Transmissionsprofile innerhalb diesem Gitter als Kristallfiberstruktur angenommen (vgl. Edelsteine: Katzenaugeneffekt beim Tigerauge). Die folgende Aufgabe ist es, anisotrope Fiberstrukturen mit der Orientierung und den Anisotropiemaßen des unterliegenden Tensorfelds zu modellieren. Dafür erstellen wir per Hauptachsentransformation (PCA) ein Eigensystem für jede Zelle des Tensorfelds und modellieren eine zugehörige Ellipsengleichung als (Transfer-/Wichtungs-) Transmissionsprofil. Folglich kann die resultierende Lichtverteilung als 2D Skalarfeld oder Polarplots für Richtungsinformation visualisiert/repräsentiert werden. Wir messen Impulsantworten des Tensorfelds mit Delta-Pulsen an jeder Position und in jede Richtung um eine uniform gesamplete Map der globalen Lichtverteilungen zu erhalten. Diese Map wird als ein globales Energieflussfeld betrachtet. Wir lassen uns von der Technik FTLE aus dem Bereich Particle Tracing der Vector Field Visualization inspirieren, indem wir den Gradient des Flussfelds der resultierenden Lichtverteilungen analysieren und visualisieren. Ähnlich wie FTLE in Vektorfeldern Gräte/Kämme/LCS detektiert, erfasst unsere Methode dieselben Strukturen, anziehende/abstoßende/sattelnde Tensorfeldlinien die häufig Schlüsselstrukturen in der Natur repräsentieren, in Tensorfeldern. Wir führen diese Größe als Global Illumination Gradient ein, der einen FTLE-verwandten Ansatz darstellt, um LCS in Tensorfeldern durch die Analyse des globalen, durch einen Imprint (Gravur in kristallinen Fiberstrukturen) gerichteten Lichtflusses, zu visualisieren. Außerdem führen wir Deformation Ellpsoid Glyphen ein, die zusätzlich zur Darstellung der anisotropen Topologie die Richtung(Zug-/Druck) der Spannung durch Pfeile nach innen/außen darstellen. Das

Verfahren wird in einer extensiven Evaluationsphase auf Plausibilität und Vergleichbarkeit geprüft.

Abstract

Tensor Fields, are most commonly associated with stress distributions (cnf. Cauchy-Stress Tensor) in 2D/3D grids, but also have some other meanings in practice in physics. By means of global illumination techniques, we develop a new method to visualize tensor fields, which is also capable of visualizing the light transport (propagation) in a topologically defined scene geometry. As a basis, we derive a simple light propagation scheme for Cartesian grids, which satisfies propagation attenuation and energy-conservation principles and is able to approximate light distributions for given light source position(s) and direction(s) until convergence. The transmission profiles within this grid are considered as crystal fiber structures as an underlying physical model (eg. gemstones: tiger's eye's cat's eye effect). The consequent task is to model anisotropic fibre structures with the orientation and anisotropy measures of the underlying tensor field in the grid. For this, we derive an eigenbasis by PCA (principal component analysis) for every cell of the tensor field and form an ellipsoid equation as transmission (transfer/weighting) function for the transmitted light profiles. Hence, the resulting light distribution can be visualized via 2D scalar field or polar plots for directional information. Additionally, We measure impulse responses of the tensor field with Delta-Pulses as light sources at any (sampled) position and in any direction to generate a uniform sampled map of the global illumination distributions. This map is considered as a global illumination energy flow field. We gain inspiration by vector field particle tracing's FTLE approach for analyzing the gradient of the flow field of the resulting light distributions. Similar to how the FTLE detects ridges/LCS (Lagrangian Coherent Structures) in vector fields (flow fields), our approach captures these structures likewise, attracting/repelling/saddling tensor field lines (TFL) which frequently represent key structures in nature, in tensor fields. We denote this entity a global illumination gradient which states an FTLE-related approach for visualizing LCS in tensor fields through analysis of the global and light transport directed by imprint/engraving in crystelline fiber structures. We also introduce Deformation Ellipsoid Glyphs which are, additionally to visualizing anisotropic topology, pointing inward/outward for compressive/tensile stresses visualizing orientation of principal mechanical stresses. We evaluate our approaches for plausibility and comparability within an extensive test campaign.

Contents

1 Introduction

In this work, we wil discuss the advantages of tensor field analysis and develop a new method for tensor field and a coherent light transport visualization. At first, we will shortly state the problem setting objectives and then give a quick overview about the structure of this work.

1.1 Motivation

Tensor Field Visualization is gaining importance as a relevant tool for the analysis of fluid and solid mechanics. Tensors are found most commonly in medical, scientific and engineering applications. A tensor is a n-D generalization of a matrix and appears e.g. as Jacobi-Matrix in Vector (Flow) Field Visualization or as stress tensor in solid continuum mechanics. Basically, tensors describe compressions, tensions, rotations and volume changes in both solid and fluid material. While most techniques focus on symmetric tensor field visualization (like Glyphs and Tensor Field Lines), some other recent works adress the problem of asymmetric tensor field visualization. The issue with asymmetric or antisymmetric tensors is that they do not always yield real eigenvalues, which is needed to determine an eigenbasis to set up glyphs, hyperstreamlines or tensor field lines. [Zheng and Pang, 2005] et.al. proposed the concept of dual eigenvectors and [Lin et al., 2012] extended it to pseudo-eigenvectors and introduced eigenvector and eigenvalue manifold to visualize eigenvectors in the complex domain. In this work, we will use the **U**-matrix obtained from singular value decomposition (SVD) to obtain the half-axes of the PCA principal ellipsoid as suggested by [Moler, 2016].

Worum geht es? Beispiel(e)! Illustrationen sind hier meist sinnvoll zum Verständnis. Warum ist das Thema wichtig? In welchem Kontext?

1.2 Objectives

The main purpose of visualization in general is to reduce or encode some set of numbers in some readable, explorable and more intuitive representation. This implies e.g. clus-
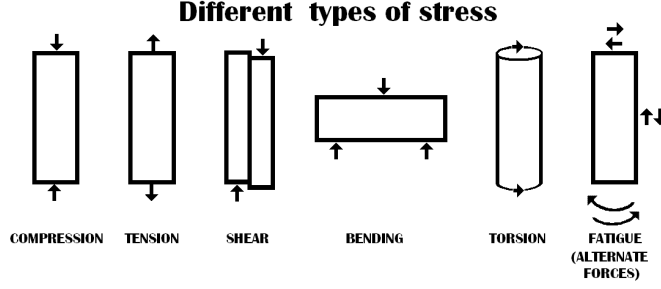
Different types of stress

Figure 1.1: Different types of stresses

tering, structuring or projection techniques. When it comes to tensor fields, this comes handy in e.g. medical sciences such as in DT-MRI (diffusion tensor-medical resonance imaging) or in simulated (or measured) stress tensor fields from solid and fluid mechanics. The problem setting encomprises the visualization of tensor fields, i.e. mostly 2D/3D-grids consisting of mainly second-order tensors (cnf. Cauchy-Stress Tensor) with the additional possibility to model light transport transport in a geometrical scene. The objective of this work is to develop a simple light propagation scheme following the most basic but crucial physical principles and laws. This propagation scheme can either be used to visualize the light transport paths (separatrices) in a geometry scenery. Or, on the other hand, be used to visualize the anisotropy characteristics of a given tensor field. Therefore the tensor field somehow needs to be pre-processed to generate a tensor-induced footprint map of transmission profiles. So however, the tensors need to be decomposed to obtain a kind of transmission profile. Another aim is to implement an approach borrowed from vector-field visualization. We construct an FTLE-related approach in tensor field visualization (both symmetric and asymmetric) for detecting ridges/LCS (Lagrangian Coherent Structures). These structures can be classified (identified) as repelling, attracting and saddling (forming a saddle) local features, which frequently represent key structures in nature. LCS usually separate regions of different flow behavior, but in our case they separate regions/domains of differing stress distributions (w.r.t. direction - measuring anisotropy/location - measuring). The map responds most where tensor field lines / hyperstreamlines converge or diverge, whereas one is the same as the other because of bidirectional stress directions. The real part of the eigenvalues can be exploited for sign change (contractions/tensions) which leads to the concept of deformation glyphs w. attached arrows pointing inward/outward for the two types of normal stresses. Practically, in its eigenbasis there are no shear stresses existent for the symmetric stress tensor in equilibrium, just the principal normal stresses. Thus, we can even define the full set of stresses with the deformation glyphs which are derived
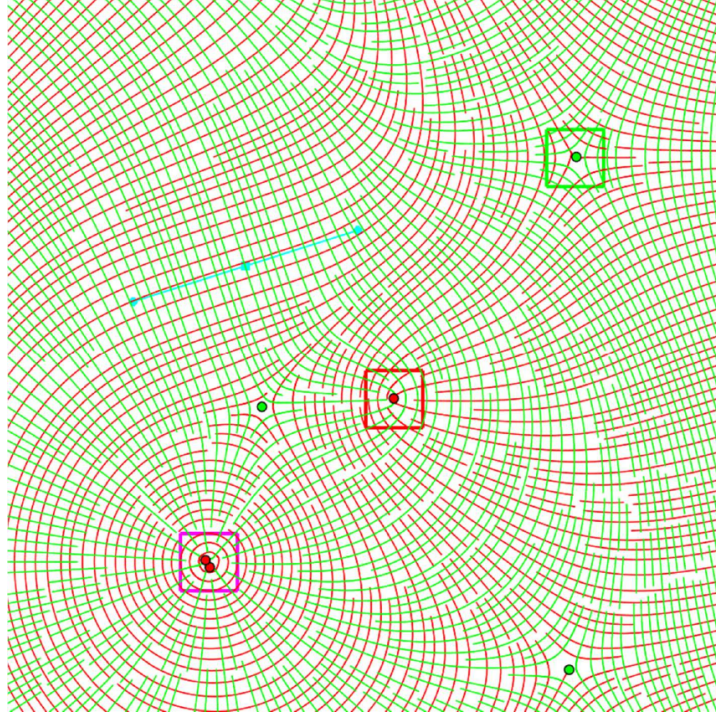
Figure 1.2: Hyperstreamlines in Tensor Field Visualization

from the singular value decomposition and signed with the real part of the eigenvalues (in corresponding absolute order).

1.3 Structure of this work

For the rest of this work, we will give a quick overview on the structure and outline. Next, in chap. 2, we will capture important fundamentals like Tensors and PCA in the context of singular value decomposition (generalization of eigenvalue decomposition). Also we will discuss the most relevant work in the domain of tensor field visualization. In chap. 3 we will propose the main contributions of this work and document the experimental evaluation in chap. 4. A compact Summary, Conclusion and Outlook will be given in chap. 5.

2 Fundamentals and Recent Work

In this chapter, we will capture the prerequisites necessary to understand the contributions of this work and will capture Tensors, PCA and Related Work in that sense.

2.1 Tensors

Now what is a Tensor? A tensor is a o-dimensional generalization of a matrix as follows:

order	0	1	2	3	...	o
shape	scalar	vector	matrix	"3D-matrix"	...	oD-matrix

Table 1: Tensor Shapes

In addition to that, a tensor has as many indices as its order o and their run length is as long as its embedded dimension n, which is equal to the rank of the tensor for full rank (or in other words the number of elements n for a nxn-matrix). Tensors follow certain transformation rules which are defined for covariant/contravariant tensors. They are most commonly obtained and defined from physical transformation equations. Hence, any o-D number array could be a tensor, but the definition holds only if the transformation rules apply to these o-D number arrays (in a sense of physical interpretation), which is mostly true for component-indexed oD number entities following matrix multiplication and transformation rules found in physics and math. In fact, tensors themselves are interpreted as a transformation which reflects an incoming direction vector (measuring e.g. the stress in that direction) to an outgoing stress vector. To be a bit more concrete, tensors represent stress distributions in solids and fluids describing strain and flow features as these entities aren't simple numbers or vectors. They occur in form of a tensor fields, and thus as entities or quantities in physics. That is, at each point in space (the grid) there is a whole distribution of e.g. stresses (elastic and viscous) which needs to be characterized and represented by a single tensor.

Cauchy stress tensor

The Cauchy stress tensor, which is propably the classical example of a tensor, is depicted in Fig. 2.1 and consists of 3 stress vectors $\mathbf{T}(\mathbf{e_i})$ arranged in row-major order.

Figure 2.1: Cauchy-Stress Tensor

It appears in similar form as viscous stress tensor in fluid mechanics:

$$
\boldsymbol{\sigma}_{ij} =
\begin{bmatrix}
\mathbf{T^{(e_1)}} \\
\boldsymbol{T^{(e_2)}} \\
\boldsymbol{T^{(e_3)}}
\end{bmatrix}
=
\begin{bmatrix}
\sigma_{xx} & \sigma_{xy} & \sigma_{xz} \\
\sigma_{yx} & \sigma_{yy} & \sigma_{yz} \\
\sigma_{zx} & \sigma_{zy} & \sigma_{zz}
\end{bmatrix}
=
\begin{bmatrix}
\sigma_{x} & \tau_{xy} & \tau_{xz} \\
\tau_{yx} & \sigma_{y} & \tau_{yz} \\
\tau_{zx} & \tau_{zy} & \sigma_{z}
\end{bmatrix}
=
\begin{bmatrix}
\sigma_{11} & \sigma_{12} & \sigma_{13} \\
\sigma_{21} & \sigma_{22} & \sigma_{23} \\
\sigma_{31} & \sigma_{32} & \sigma_{33}
\end{bmatrix}
$$

These 3 stress vectors represent the orientation and magnitude of total resulting stress at plane x, y, z in direction x, y, z (9 individual numbers). Thus, the stress tensor poses a full valid represenation of the stress distribution at any point in space. The stress tensor itself can be interpreted as a transformation which maps an incoming normal direction vector $\mathbf{n}$ a resulting stress vector $\mathbf{T^{(n)}} = \mathbf{n} \cdot \boldsymbol{\sigma}$. The stresses in normal directions (diagonal elements) are directly related to the pressure, which is always isotropic and hence non-directionally dependent. It is possible to find 3 principal stress directions in 3D through PCA (see sect. 2.2 below), for which there are no shear stresses existent in equilibrium. These form the principal directions of deformation at a certain location and are sufficient to describe the resulting transformation/deformation behaviour. The resulting system of principal directions and absolute stresses is often called an "eigensystem" or "eigenframe". So to say, an eigensystem, consistent of the principal directions/axes, spans a principal ellipsoid depicted in Fig. **??** in sect. 2.2.

2.2 Principal Component Analysis

Note that we denote a matrix as a second order tensor interchangeably for the sake of simplicity in the following. For any state of stress in equilibrium it is possible to find n (dimensionality) independent orthogonal directions with no shear stresses existent. Along these directions the principal stresses, which are normal (tensile/compressive) stresses, are exerted. The anisotropy can be represented by e.g. ellipsoid glyphs.
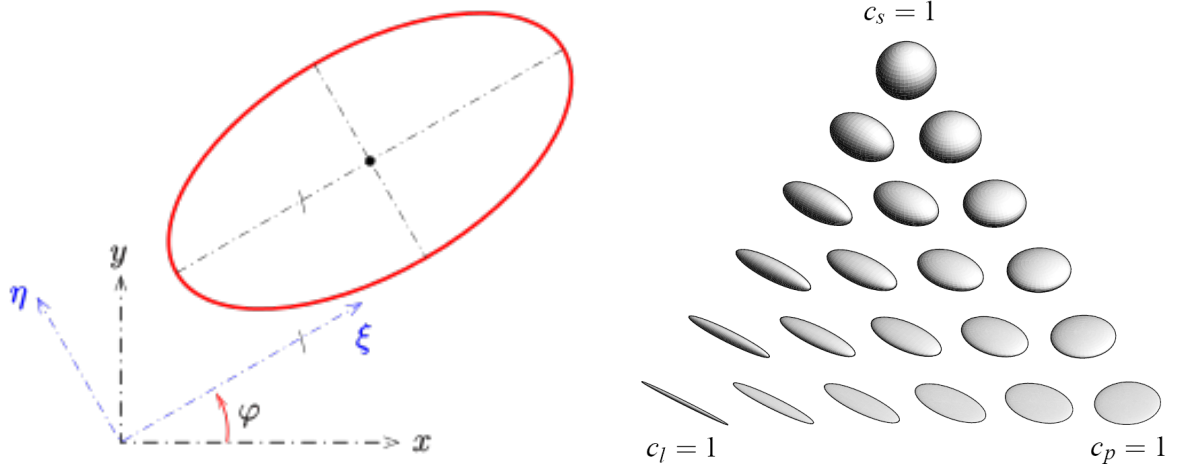

Figure 2.2: a) Principal Component Analysis, b) Ellipsoid Glyphs w. anisotropy coefficient (l:linear, p:planar, s:spherical)

Principal Component Analysis is an algorithm which can capture the principal components (directions) in stochastic data. But it works similarly on transformations to capture the principal directions from transformations like rotation and scaling. Now, principal component analysis can be done by eigenvalue or singular vector decomposition, whereas the former yields complex eigenvalues for asymmetric matrices. For (skew-)symmetric (normal) matrices, they are connected through the following relation: $s_i = \sqrt{|\lambda_i|}$ (cnf. [Kieburg, 2016]). Note that the eigenvectors match the singular vectors only for symmetric matrices, which does not mean that they do not form the half-axes of the principal component ellipsoid in other cases. Mathematically speaking, a decomposition is somehow decomposing a transformation (which follows certain transformation rules) into parts of subsequent transformations consistent of rotation and scaling ($\mathbf{A} = \mathbf{RSR}^*$). We choose to use singular value decomposition ($\mathbf{A} = \mathbf{U\Sigma V}^*$) to be able to set up real eigenvalues for any kind of matrix (singular values are always real and positive). Also, the singular vectors of the $\mathbf{U}$-matrix represent the half-axes of the principal ellipsoid (eigenframe) shown in Fig. **??** for any kind of matrix as pointed out by [Moler, 2016]. In addition, we also calculate the eigenvalues to exploit the sign

of the real part of the eigenvalues ([Mroz, 2016]) ordered decreasingly by absolute value (corresponding to singular value order). The sign corresponds to tensile (+) and compressive (−) stress, which would allow us to visualize deformation glyphs with arrows pointing inwards for compressive and outwards for tensile stresses. We do this decomposition analysis once for each matrix and then store the precomputed results in a grid. The principal ellipsoid is also used as a transmission profile for the propagation scheme in symbolic form in a subequent step. In this work, we will use the singular vectors yielded from singular value decomposition to avoid complex values yielded from eigenvalue decomposition. This will allow us to set up glyphs representing the major/minor axis of the underlying transformation for every kind of (asymmetric/symmetric) tensor. We will then use global-illumination techniques on top to generate a flow map, which permits us to compute an FTLE-like field on the tensor fields.

2.3 GT Algorithms / Approaches

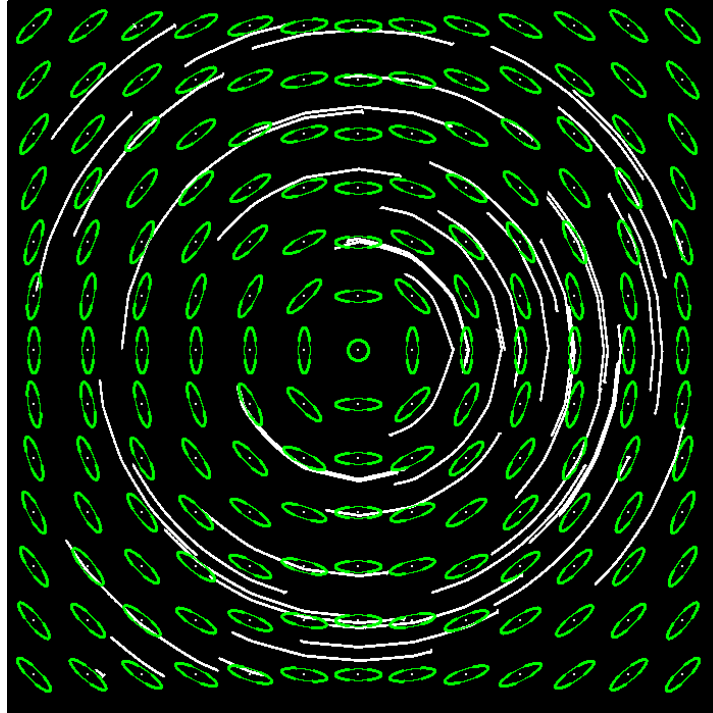### 2.3.1 Glyphs and Tensorfieldlines

Figure 2.3: white: Tensorfieldlines; green: Ellipsoid Glyphs

Glyphs were derived as a basis for the weighting profiles of the tensors in the following propagation scheme. They were chosen because it is an easy-to-use (understand) concept

which can also be interpreted nicely. In fact, these are used for the principal component analysis of direction vectors for the Tensor Field Line extrapolation (integration) in a subsequent step. Tensor Field Lines (the type of tensor stream line - hyperstreamline analog that does not introduce artificial intertia) were implemented for Ground Truth (GT) data generation purposes. For example, when we design an FTLE-like field computation approach, we will need to know when tensor field lines diverge/converge.

2.3.2 Test Data (Generation)

We used python's numpy library to generate pre-defined test cases and caught one real data example from `TensorVis.org`, which needed to be pre-processed through slicing and subsequent cropping to 2D samples (2x2 matrices), which can be grouped into symmetric and asymmetric ones:

Symmteric Tensor Fields

   Asymmteric Tensor Fields

2.4 Related Work

There has been extensive recent work on symmetric tensors but in comparison little on asymmetric ones. Since we aren't able to cover the whole scope in this work, we will focus on the most relevant works about tensor field visualization.

   Symmetric Tensor Field Visualization

[Zheng and Pang, 2005] et.al. proposed a texture-based visualization approach called HyperLIC, which extends the concept of LIC to symmetric tensor fields by using an anisotropic 2D-filter kernel oriented along the major/minor eigenvectors. The concept of following the major/minor eigenvector along tensor field lines was invented by [Vilanova et al., 2004]. Tensorlines introduce a kind of artificial inertia (running average), making them resistent to noise. The notion of tensor field topology and the concept of Hyperstreamlines was first introduced by [Delmarcelle and Hesselink, 1995]. The placement of tensor field lines as hyperstreamlines was recently improved by [Spencer et al., 2009] et.al. for glyph packing. A good overview of seeding strategies is given by [**?**]. [Feng et al., 2008] et. al. used Voronoi Tesselation for placing the glyphs. Superquadric glyphs have been proposed by [Schultz and Kindlmann, 2010] for general (non-positive definite) tensors. [de Leeuw and van Wijk, 1993] visualize the partial derivative gradient, the Jacobian of the tensor field to sense the local properties of the field. A diffusion tensor can also be visualized by box [A. Worth, 2016], ellipsoid [Pierpaoli and Basser, 1996], composite [**?**] or superquadric [Kindlmann, 2004] glyphs. There is also a set of scalar measures available

in symmetric tensor field visualization such as: mean diffusivity, fractional anisotropy [Basser, 2011] and anisotropy coefficients [Westin et al., 1997]. [Hlawatsch et al., 2011] et.al. obtain a coordinate (flow) map from tensor field lines following major/minor eigenvectors (fibre trajectories) and use the spectral norm of the Cauchy-Green deformation tensor to compute the FTLE-field in homogeneous regions. In a similar manner, we opt to use Global Illumination Techniques to obtain a light distribution footprinted (in form of weighting profiles obtained from ellipsoid glyphs) by the tensor field.

Asymmetric Tensor Field Visualization

[Zheng and Pang, 2005] et.al. proposed the concept of dual eigenvectors and [Lin et al., 2012] extended it to pseudo-eigenvectors and introduced the eigenvector/eigenvalue manifolds to visualize eigenvectors in the complex domain. [Palke et al., 2011] et.al. focused on the efficient implementation and visualization of these structures and provided an interactive visualization system for asymmetric tensors applicable in fluid and solid dynamics. The concept of Tensor Magnitude has been introduced by [**?**] for means of physical interpretation. They also proposed an efficient glyph and hyperstreamline hybrid approach, which made dynamic interaction in real-time in 2D tensor fields feasible. [Palacios et al., 2015] extracted isosurfaces of tensor magnitude, mode and isotropy index.

Typischerweise im letzten Abschnitt dieses Kapitels wird dann auf verwandte Arbeiten eingegangen. Entsprechende Arbeiten sind geeignet zu zitieren. Beispiel: Die wurde erstmalig in den Arbeiten von Spitz und Gertz [**?**] gezeigt ... Details dazu werden in dem Buch von Newman zu Netzwerken [**?**] erläutert ....

3 Main Part

This chapter will summarize the main contributions of this work studied and state targeted aims and goals as a first step in sect. **??**. Then we will have a short introduction to the implemented global illumination scheme derived and simplified from an nVidia GI approach in sect. 3.2. Last, we will state the effectively developed Visualization methods GIGradient and Deformation Glyphs proposed as innovatively invented tensor visualization techniques.

3.1 Requirements and Ambitions

Our ambition is to develop a simple and efficient Global Illumination Propagation Scheme able to distribute energy profiles in discrete polar form in 2D/3D-space w.r.t. energy conservation and propagation attenuation principles. We then generate transmission profiles from the eigensystems (principal component frames) of the tensors for each cell in the domain (field). That is, to provide an orientation for a grid of crystal fibre structures (cnf. optical fibres) to redirect the intensities in analogy to the anisotropies of the tensor field within a glyph representation, obtained from Principal Component Analysis. Our approach should be implicitly adaptive to any kind of 2D dataset. Thus, we opt to be compatible to handle any kind of matrix (symm./anti-symm.) and any kind of resolution of the field (full-spectrum). At last, we aim to generate a new FTLE-related method for tensor field visualization by applying a Global Illumination Gradient to the resulting light distributions for every possible position and direction of the light source in the grid generated by stimulation with Delta-Impulses. Thus, our motivation is to segment key locations (LCS/ridges) in the field with tensor field lines (hyperstreamlines) converging/diverging, which is necessarily the same (for bidirectional tensor fields). Our approach should efficiently handle (relatively) large datasets.

3.2 Global Illumination (Propagation) Scheme

Within the scope of this work, we will develop a Global Illumination Scheme designed to efficiently propagate the intensities stored in discrete polar coordinates given as impulses

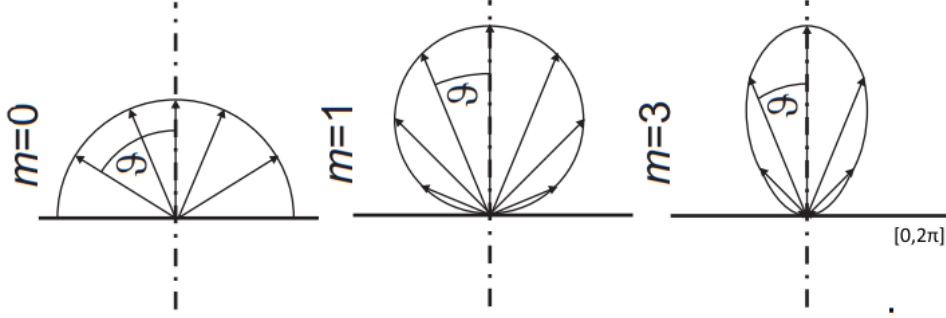(stimuli) by the user or the config. Polar profiles for different light sources are shown in Fig. 3.1:

Figure 3.1: Polar Profiles for Different Types of Emitters

As a reminder, polar profiles map each angle φ a magnitude r forming a function $r(\varphi)$. They are circular axis versions of the domain $[0..2\pi]$, with negative magnitudes mirrored by 180 degrees). Thus, they are functions with an angular domain making them directionally dependent, which is a well suited representation for point lights, as we use them in a style of [Kaplanyan and Dachsbacher, 2010] et.al. For the sake of interpretability, we exclude negative values (energies) from the scope of our calculations. As a start-up thinker for the propagation scheme, we will think of a grid cell in 2D as a center pixel within an 8-neighborhood. Remember, that all considerations from now on are given concerning a single grid cell respectively. It has 8 (4 faces/edges and 4 diagonals) unique neighbors, which are adjacent point lights in the grid (the type of light source with theoretically no finite extend). We consider one face neighbor (top) to shortly explain the steps of the scheme. The diagonals and the others are obtained from derivation and symmetry.

Each cone (yellow and green) is an individual neighbor-dependent angular area. We optimize for distributing contributions for overlapping cones to transmit attenuated (because of the larger factor $\sqrt{2}$ distance) intensity in form of a shared part to the diagonals in a single step. Therefore, the intensity gathered in polar coordinates in areas marked in green, need to be partitioned between 2 of the 8 cone-index neighbors with following consideration:

The face neighbors take in the angular domain of $d_1 = \alpha + 2\beta$, whereas the diagonal neighbors span a domain of $d_2 = 2\beta$. The linear combination weights for the overlapping (green) parts (β) are obtained from the relative overlapping angular area of the angular span β w.r.t. diagonal cones (2β) and face cones ($\alpha + 2\beta = 90°$) (yellow cone is overlapped by green cones at full angle). The linear combination weights are subsequently
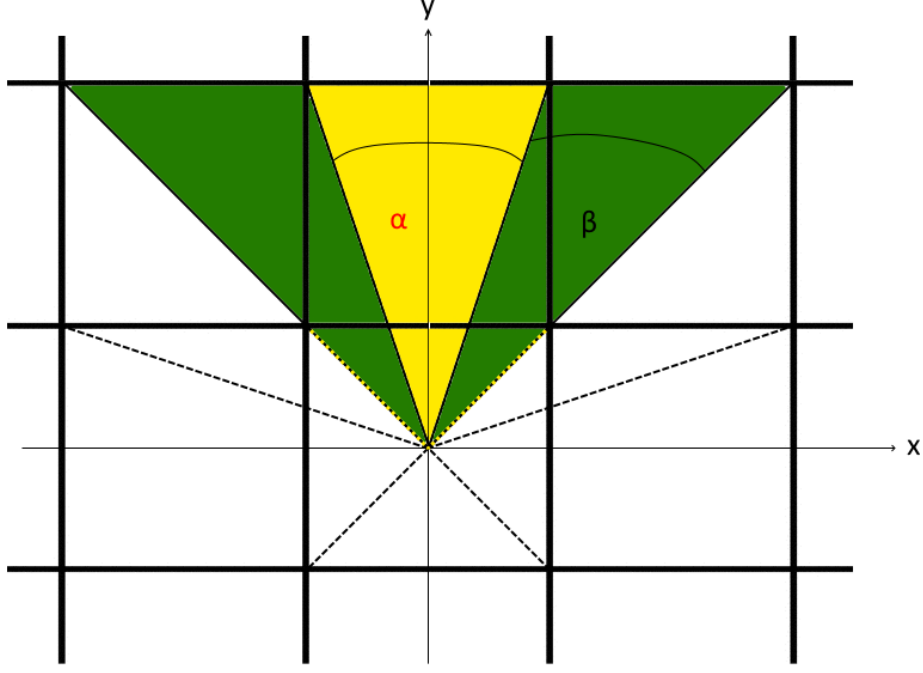
Figure 3.2: Propagation Scheme

normalized to $\sum = 1.0$ (normalization condition):

$$\varepsilon_1 = \frac{\frac{\beta}{\alpha+2\beta}}{\frac{\beta}{\alpha+2\beta} + \frac{\beta}{2\beta}} \approx 0.362291 \tag{3.1}$$

$$\varepsilon_2 = \frac{\frac{\beta}{2\beta}}{\frac{\beta}{\alpha+2\beta} + \frac{\beta}{2\beta}} \approx 0.63771 \tag{3.2}$$

We place a cosine lobe scaled with the integrated (accumulated) energies in each of the 8 cone directions, whereas outgoing integrated and summed energies are weighted by the linear combination weights (factors) in overlapping (green) areas to split up the contributions accordingly. The contribution areas are depicted in Fig. 3.2, the cosine lobes can be observed in Fig. 3.3 respectively. This manner of propagation is inspired by the propagation scheme of [Kaplanyan and Dachsbacher, 2010] et.al. (see the paper on how to "project the flux into a point light"). The implementation is done in a dual buffer approach which pushes the energies back and forth (buffer A to buffer B) until convergence, which happens when the energy is spreaded throughout the grid and enters a stationary state, characterized by equal out (at grid borders) to in (at light source positions) energy-flow with no more nettings going on inside the domain. Note that even though we propagate the energy directly through the diagonal cones (which forms

a square initially), the 8 degrees of freedom introduce a circular (spherical) wave front after few iterations (for greater resolutions) as depicted in Fig. 3.3. This occurs, since the diagonals are more strongly attenuated by default and there is a redistribution of intensities in the long term resulting in a circular torus-shaped distribution, as observed in Fig. 3.3. Also note, that this approach satisfies energy conservation and propagation attenuation principles and applies to the principles of light propagation in vacuum (by default). The verification of these principal requirements and specifications can be observed in the Experimental Evaluation in chap. 4.

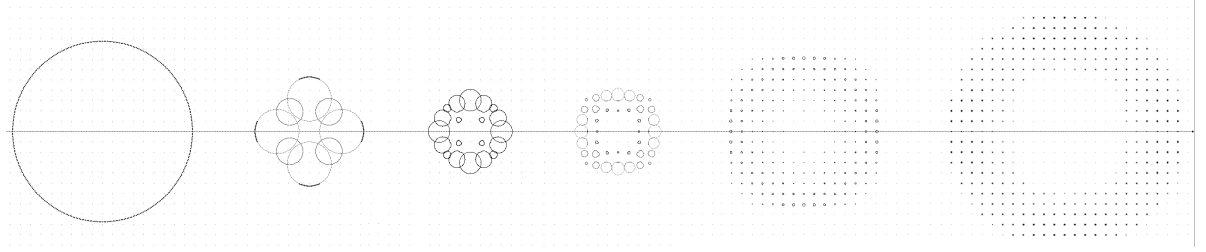We show a few of the first iteration steps for the propagation scheme in Fig. 3.3:

Figure 3.3: Impulse Response for Isotropic Stimulus (Few Iterations: 0,1,2,3,7,11)

It can be proven that the approach follows propagation attenuation principles and follows the inverse (square) law ($\sim \frac{1}{r}$) as observed in the graph in Fig. 3.4.
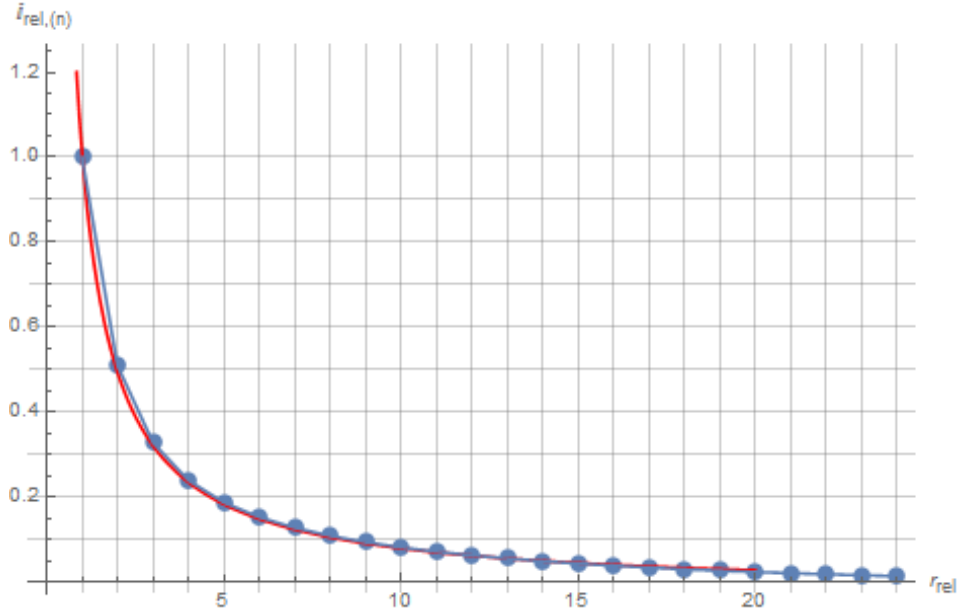

Figure 3.4: Propagation Attenuation

At last, we define a threshold for the minimum overall distribution error taken into

account for convergence conditions, initiating a stop sequence when falling below that threshold. As already mentioned, a dual-buffer approach is chosen here, as we can efficiently propagate from one into the other and just swap pointers to start all over (after reinitialization). Another reason is it yields a reasonable source-target structure. We introduce a new operator called *propagate*, which we will fill with meaning in sect. 3.3 in form of a precise mathematical formulation. Each Grid or Buffer is basically a set of cells defined as $\mathcal{C} = \{\mathbf{c}_1, \mathbf{c}_2, ..., \mathbf{c}_n\}$ The dual buffer result $\mathcal{C}'$ is denoted symbolically as follows for all cells w. a mean intensity greater than zero (which do not contain Null samples):

$$\mathcal{C}' = propagate\{c_i \in \mathcal{C} \mid |\bar{I}_i| > 0\} \ w. \ i = \{1..dim\} \tag{3.3}$$

Note that, $dim = width \cdot height$, which equals the tensor field resolution in this case.

Until now, we aimed to simulate the propagation of light in empty space (vacuum) providing us with a physically-motivated but very simplified base-approach. We aim to modulate the transmission of the energies on top of the base approach with transmission profiles obtained from the tensor fields through Principal Component Analysis and ellipsoid glyph equations in the following.

3.3 Transmission Profiles and Weighting Functions

To obtain a kind of footprint of the tensor field, we set up ellipse equations for each glyph representation, obtained from applying PCA on each cell (tensor) in the field. We map the singular values (corresponding to eigenvalues) in decreasing order to the ellipses radii (half-axes) $a(\lambda_1)$ and $b(\lambda_2)$ as follows:

Ellipse Equation:

$$r(\omega) = \frac{ab}{\sqrt{a^2 \sin^2(\omega - \varphi) + b^2 \cos^2(\omega - \varphi)}} = \frac{\lambda_1 \lambda_2}{\sqrt{\lambda_1^2 \sin^2(\omega - \varphi) + \lambda_2^2 \cos^2(\omega - \varphi)}} \tag{3.4}$$

That is, the singular values form the half-axes of the PCA ellipsoid, which yields us a symbolic definition for our transmission (transfer) function as weighting profiles. We compute the offset angle φ w.r.t. x-axis by exploiting the atan2-function with 4-quadrant evaluation for the first singular vector. As a preliminary prep, this profile is precomputed (sampled) for all discrete angular steps for each cell (e.g. 360). The weighting scheme which we apply is depicted in Fig. 3.5. We interpret the polar functions as discrete, sampled 1D vectors with a constant angular resolution. That means, we use element-wise multiplication for the 1D-vectors in red (Intensity Profile) and cyan (Transmission
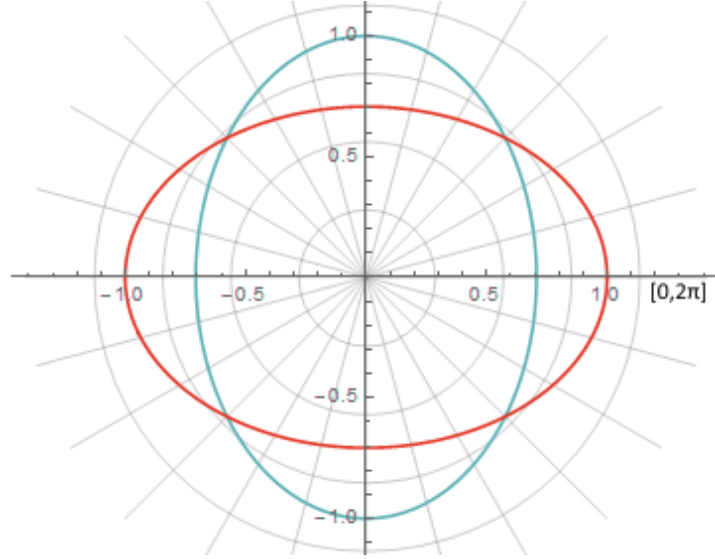
Figure 3.5: red: Intensity Profile, cyan: Transmission Profile (Glyph Ellipsoid Eq.)

Profile) to obtain a windowed version of the intensity profile and perform the following integration step to accumulate the total radiant power (flux) as follows. Note that we model angular dependent radiant intensity $I(\omega)[\frac{W}{rad}]$ as an underlying physical entity, which is well suited for describing point light sources. As a side note, the physical quantity perceived as brightness by human eyes, is the radiance (luminance), which is yielded by relating radiant intensity to a finite sensitive area ($[\frac{W}{rad}/m^2]$). The primary definition for our total accumulated incident radiant flux is denoted as:

$$\Phi_t = \int_0^{2\pi} I(\omega)T(\omega)\,d\omega \tag{3.5}$$

$$\sum_{\cos} = \int_0^{2\pi} \cos(\omega)\,d\omega \approx 2 \tag{3.6}$$

This enables us to scale an oriented cosine-lobe w. the total radiant flux w. respect to its own total energy when integrated likewise. A discrete cosine lobe never reaches its theoretical sum of 2 exactly in the interval $[0, 2\pi]$. Therefore it needs to be computed to account for floating-point precision errors and normalized by following relation (e.g. $\sum_{\cos} \approx 1.9949204635834517$).

$$\cos_n(\omega) = \frac{\Phi_t}{\sum_{\cos}}\cos(\omega) \tag{3.7}$$

This yields a cosine lobe, which has an overall energy of Φ_t if the point light is interpreted with a Lambert-Emitter (cnf. [?]) characteristic (as part or area element of a diffusely

15

reflecting surface).

Now each tensor ellipse equation has a mean transmission rate [%], which turns out to be a measure or synonym for the total transmitted rate of the total incoming radiant intensity $\int_0^{2\pi} I(\omega)\,d\omega$. Since energy can not be generated from transmission profiles (only transmitting, not generating), we have to normalize every tensor ellipse equation with the highest mean transmission rate in the field. This restricts the tensor ellipse mean to a maximum of 100% for the one with the highest tensor magnitude. We will use the definition of mean tensor magnitude $\bar{r}_{max}$ obtained from the PCA here for simplicity. Hence the tensor ellipse equations are normalized through the following step:

$$r_n(\omega) = \frac{1}{\bar{r}_{max}} r(\omega) \tag{3.8}$$

Notice, that this implements the concept of absorption implicitly, because tensors with a lower mean $\bar{r}$ than 100% lose energy wheras absorption equals $\mu = 1 - \bar{r}$ here. Now that we have coped with the problem of overall transmission, we are left with another problem that occurs with the weighting functions as that they can yield values above 1.0. This would potentially generate intensity out of nothing which leads to crucially unstable behaviour. Well, but only in case energy conservation principles were not respected. To construct a solution, we ask for the source of the excessive energy. If the tensor mean complies with the constraint $\bar{r} \leq 1.0$, then the energy must lack in some other place (since the overall transmission fulfills the energy conservation constraint in that case). The only problem is that a normalization condition in usual style for the transmission profile $T(\omega)$ does not necessarily imply the same normalization for the term $I(\omega)T(\omega)$. However, a proper normalization can give corrective remedy, wich reveals another subsequent normalization constraint. The normalization factor is defined in 3 subsequent steps:

1. Normalization of TI to $\overline{TI} = 1.0$

2. Subsequent scaling w. mean intensity $\bar{I}$ for energy conservation principles

3. Subsequent scaling w. mean tensor magnitude $\bar{T}$ for absorption principles

Hence the transmitted energy is given as:

$$I_t(\omega) = n_f I(\omega) T(\omega) \qquad w.\ n_f = \frac{\bar{T}\bar{I}}{\overline{TI}} \tag{3.9}$$

This transforms our equation for the radiant flux into:

$$\Phi_t = \int_0^{2\pi} I_t(\omega) T(\omega) \, d\omega \tag{3.10}$$

Which is now respecting energy conservation principles very conveniently, as all we need is a set of means and we are done.

This approach ensures that no energy will be generated and therefore implements the physical law of energy conservation or Kirchhoff's current law if you want to think of a particle's diffusion process. Consequently, this allows us to assume that all sources of power (energy) are user-defined. In fact the approach has proven to be robust w.r.t. energy losses for several iterations as depicted in chap. 4 in the stochastic error graph.

3.4 Physical Model

3.5 Global Illumination Gradient

Note that the resulting scalar field is $(n + 1)$-dimensional (x, y, z and direction θ) and needs to be flattened by averaging or projection in 3D for proper visualization. Usw.

4 Experimentelle Evaluation

Der Aufbau dieses Kapitels oder dessen Aufteilung in zwei Kapiteln ist stark von dem Thema und der Bearbeitung des Themas abhängig. Beschrieben werden hier Daten, die für eine Evaluation verwendet wird (Quellen, Beispiele, Statistiken), die Zielsetzung der Evaluation und die verwendeten Maße sowie die Ergebnisse (u.a. mithilfe von Charts, Diagrammen, Abbildungen etc.)

Dieses Kapitel kann auch mit einer Beschreibung der Realisierung eines Systems beginnen (kein Quellcode, maximal Klassendiagramme!).

5 Zusammenfassung und Ausblick

Hier werden noch einmal die wichtigsten Ergebnisse und Erkenntnisse der Arbeit zusammengefasst (nicht einfach eine Wiederholung des Aufbaus der vorherigen Kapitel!), welche neuen Konzepte, Methoden und Werkzeuge Neues entwickelt wurden, welche Probleme nun (effizienter) gelöst werden können, und es wird ein Ausblick auf weiterführende Arbeiten gegeben (z.B. was Sie machen würden, wenn Sie noch 6 Monate mehr Zeit hätten).

Bibliography

[A. Worth, 2016] A. Worth, N. M. (2016). Fusion of MRI data for visualization of white matter bundles. `http://neuromorphometrics.org/papers/Worth/WorthMICCAI98reject.pdf`. [Online; accessed 22-05-19].

[Basser, 2011] Basser, P. (2011). Microstructural and physiological features of tissues elucidated by quantitative-dicusion-tensor mri. *J Magn Reson*, 213:560–570.

[de Leeuw and van Wijk, 1993] de Leeuw, W. C. and van Wijk, J. J. (1993). A probe for local flow field visualization. In *Proceedings Visualization '93*, pages 39–45.

[Delmarcelle and Hesselink, 1995] Delmarcelle, T. and Hesselink, L. (1995). Visualizing second order tensor fields with hyperstreamlines.

[Feng et al., 2008] Feng, L., Hotz, I., Hamann, B., and Joy, K. (2008). Anisotropic noise samples. *IEEE Transactions on Visualization and Computer Graphics*, 14(2):342–354.

[Hlawatsch et al., 2011] Hlawatsch, M., Vollrath, J. E., Sadlo, F., and Weiskopf, D. (2011). Coherent structures of characteristic curves in symmetric second order tensor fields. *IEEE Transactions on Visualization and Computer Graphics*, 17(6):781–794.

[Kaplanyan and Dachsbacher, 2010] Kaplanyan, A. and Dachsbacher, C. (2010). Cascaded light propagation volumes for real-time indirect illumination. In *Proceedings of the 2010 ACM SIGGRAPH Symposium on Interactive 3D Graphics and Games*, I3D '10, pages 99–107, New York, NY, USA. ACM.

[Kieburg, 2016] Kieburg, M. (2016). What is the Relation between Eigenvalues & Singular Values? `http://wt.iam.uni-bonn.de/fileadmin/WT/Inhalt/people/Patrik_Ferrari/Conference2016/TalkKieburg.pdf`. [Online; accessed 22-05-19].

[Kindlmann, 2004] Kindlmann, G. (2004). Superquadric tensor glyphs. In *Proceedings of the Sixth Joint Eurographics - IEEE TCVG Conference on Visualization*, VISSYM'04, pages 147–154, Aire-la-Ville, Switzerland, Switzerland. Eurographics Association.

[Lin et al., 2012] Lin, Z., Yeh, H., Laramee, R., and Zhang, E. (2012). 2d asymmetric tensor field topology.

Bibliography

[Moler, 2016] Moler, C. (2016). Numerical Computing With MAT-LAB, 2004 / Bug Report Revives Interest in SVD Option of ?Eigshow? `https://blogs.mathworks.com/cleve/2016/08/08/bug-report-revives-interest-in-svd-option-of-eigshow/`. [Online; accessed 22-05-19].

[Mroz, 2016] Mroz, L. (2016). What is the Relation between Eigenvalues & Singular Values? `https://www.cg.tuwien.ac.at/research/vis/seminar9596/2-topo/evinter.html`. [Online; accessed 22-05-19].

[Palacios et al., 2015] Palacios, J., Yeh, H., Wang, W., Zhang, Y., Laramee, R., Sharma, R., Schultz, T., and Zhang, E. (2015). Feature surfaces in symmetric tensor fields based on eigenvalue manifold. *IEEE transactions on visualization and computer graphics*, 22.

[Palke et al., 2011] Palke, D., Lin, Z., Chen, G., Yeh, H., Vincent, P., Laramee, R., and Zhang, E. (2011). Asymmetric tensor field visualization for surfaces. *IEEE Transactions on Visualization and Computer Graphics*, 17(12):1979–1988.

[Pierpaoli and Basser, 1996] Pierpaoli, C. and Basser, P. J. (1996). Toward a quantitative assessment of diffusion anisotropy. *Magnetic resonance in medicine*, 36 6:893–906.

[Schultz and Kindlmann, 2010] Schultz, T. and Kindlmann, G. L. (2010). Superquadric glyphs for symmetric second-order tensors. *IEEE Transactions on Visualization and Computer Graphics*, 16(6):1595–1604.

[Spencer et al., 2009] Spencer, B., Laramee, R. S., Chen, G., and Zhang, E. (2009). Evenly spaced streamlines for surfaces: An image-based approach. *Comput. Graph. Forum*, 28:1618–1631.

[Vilanova et al., 2004] Vilanova, A., Berenschot, G., and van Pul, C. (2004). Dti visualization with streamsurfaces and evenly-spaced volume seeding. In *Proceedings of the Sixth Joint Eurographics - IEEE TCVG Conference on Visualization*, VISSYM'04, pages 173–182, Aire-la-Ville, Switzerland, Switzerland. Eurographics Association.

[Westin et al., 1997] Westin, C.-F., Peled, S., Gudbjartsson, H., Kikinis, R., and Jolesz, F. A. (1997). Geometrical diffusion measures for MRI from tensor basis analysis. In *ISMRM '97*, page 1742, Vancouver Canada.

[Zheng and Pang, 2005] Zheng, X. and Pang, A. (2005). 2d asymmetric tensor analysis. pages 3– 10.